Effects of AC Dielectric Barrier Discharge plasma actuator location on flow separation and airfoil performance

Yann Bouremel[*1], Jiun-Ming Li[1], Zijie Zhao[2] and Marco Debiasi[1]
[1]Temasek Laboratories, National University of Singapore, Singapore
[2]Department of Mechanical Engineering, National University of Singapore, Singapore
[*] Email: tslyb@nus.edu.sg

Abstract

The goal of this work is to characterize the effect of Dielectric Barrier Discharge (DBD) plasma actuator on the lift and drag coefficients generated by the flow around a NACA 4415 airfoil model using force-balance and Particle Image Velocimetry (PIV) measurements. DBD actuators have been mounted at the leading edge, at 30% and at 60% of the chord length. The effect on the airfoil lift and drag of actuation at these different locations has been studied. It has been found that for increasing angles of attack, the actuators need to be located closer to the leading edge and in front of the separation area to produce the best lift or drag coefficient improvements. If located within the flow separation zone, their effects on the airfoil lift and drag coefficients are limited.

Keywords: Dielectric Barrier Discharge Plasma, Particle Image Velocimetry, Vorticity, Force Balance Measurements, Lift Coefficient, Drag coefficient, Separation Point

1. Introduction

Several studies have demonstrated the ability of plasma actuators in active flow control. A review of Moreau [1] describes the topic of airflow control by non-thermal plasma actuators. This paper shows the recent knowledge concerning the electric wind induced by plasma actuators in quiescent air at atmospheric pressure. It also presents some active flow control applications by plasma actuators, and the effective results obtained for low-velocity airflows. In the work by Jolibois et al. [2], a study of airflow separation control above a NACA0015 airfoil by using seven DBD plasma actuators is presented. In this study, the velocity is 6 m/s, corresponding to $Re = 0.4 \times 10^6$ based on a chord length of 1 m and the plasma actuators are placed on the upper surface from $x/c = 0.3$ to 0.78. The results show that this type of action is able to reattach a naturally detached airflow or to detach a naturally attached airflow. Control of flow separation over a flap of a high-lift airfoil using a single DBD plasma actuator has also been investigated [3]. The actuator is found to be most effective for increasing lift when operated in an unsteady fashion at the natural oscillation frequency of the trailing edge flow field. According to Little et al. [3], the possible mechanism is that free stream momentum is entrained into the separated region because of natural instabilities being amplified by the actuator hence reducing the size of the time averaged separation. Plasma actuators can also be mounted at the trailing edge of the airfoil to alter the overall circulation around the airfoil thanks to Coanda effect [4]. The current novel study is motivated to look into the relation between the position of the actuator on the airfoil relatively to the flow separation point and its effect on the drag and lift by combining flow visualization and force balance measurements.

2. Experimental set-up

Three DBD plasma actuators are mounted on a NACA 4415 airfoil model respectively at the leading edge, at 30% and at 60% of the chord length. The airfoil model is made of Plexiglas with a chord c of 100 mm and a span b of 158 mm. The actuators are made of 0.066 mm thick copper, the exposed electrode located at the leading edge is a baseline

electrode while the two located downstream have a comb-like exposed electrode configuration. The dielectric between the exposed electrode and the buried electrode are made of PCB support of 1 mm thickness and two layers of Kapton sheet of 125 μm and 76.2 μm. Each actuator has been independently driven to look at the relation between its position and the lift generated when it is turned on. The peak-to-peak voltage applied to the electrodes is 15.5 kV at a frequency of 5 kHz. The experiments have been conducted at Re = 35000 based on the chord length of 0.1 m and a velocity of 5 m/s. The model was mounted on a turntable incorporating a balance. The model angle of attack α varied from -6° to 16°. The balance used to record the data is an ATI Mini40 piezoelectric gauge. Two axes were aligned with the streamwise and the vertical directions of the wind tunnel to measure the drag and the lift forces generated by the model. The recording sequence consists of 2 seconds with no actuation to define the baseline flow followed by 4 seconds with actuation. The sampling frequency was 1 kHz and the signal was low-pass filtered at 10 Hz before average in order to remove the effects of small vibrations induced by the flow. Flow-field velocity measurements were obtained by using a two-velocity-component Particle Image Velocimetry (PIV) system. The flow was uniformly seeded upstream of the wind-tunnel air intake with olive oil particles from a Dantec 10F03 seeding generator. Droplets were produced in the average size Sauter mean diameter (SMD) 2-5 μm whose reflections correspond to no more than 3 pixels in the captured images, which allow a good resolution of the particle displacement when cross-correlation methods are adopted. A dual-head Litron DualPower 200-15 Nd:YAG laser operating at the second harmonic (532 nm) at approximately 150 mJ per pulse was used in conjunction with sheet-forming optics to form a thin sheet (~1 mm) on the x-z plane passing through the centerline of the test section. The images were acquired using double frame mode by a 2048 x 2048 pixels HiSense 620 camera with a Zeiss 50 mm f/2.0 macro lens (178.3 x 178.3 mm field of view). The resulting resolution is approximately 87 μm per pixel. The camera viewed the streamwise laser sheet orthogonally over the entire field of view. To retain a good resolution of the flow particles close to the upper surface of the model, a 527 to 537 nm band-pass optical filter was placed in front of the lens whereas the surface of the model exposed to the laser sheet was sprayed with clear acrylic paint containing rhodamine 6G (which fluoresces close to 566 nm when excited by 532 nm light). A computer with dual Intel Core processors was used for data acquisition. The acquired frames were divided into 32 x 32 pixel interrogation windows, which contain at least 3 seeding particles each. Based on the flow velocity and the size of the interrogation area, the time separation between the two laser flashes (double frame mode) was set such that the maximum displacement of a particle is no more than 25% of the interrogation size which is the optimum displacement for the Dantec software to calculate accurately the particle velocity. For each frame, subregions were adaptatively cross-correlated using multi-pass processing with a final 50% overlap that gives a final interrogation area of 16 x 16 pixels after processing. The resulting vector fields were post-processed to remove remaining spurious vectors. This arrangement gives a velocity vector grid of 127 x 127 points, which translates to velocity vectors separated by about 1.39 mm over the field of view. For each acquisition, 200 velocity-vector images were taken for statistical averaging at a trigger rate of 7 Hz for the baseline flow and the experiments with the actuator switched on were repeated 4 times for statistical averaging.

3. Results and Discussions

3.1 Force balance measurements

Force measurements were used to characterize the lift and drag coefficients when the actuators located along the airfoil were switched on one by one. The goal is to find which DBD plasma actuator produces the best lift and drag coefficients for a given angle of attack and to check whether there is a correlation between the position of the actuator and the angle of attack. Figures 1 (a)-(b) show the variations of the lift coefficient C_L and the drag coefficient C_D with α when the 1st, 2nd and 3rd actuators are switched on for Re =

35000. The 1st actuator is the leading edge one (black line) while the 2nd (red line) and the 3rd actuator (green line) are located at 30% and 60% of the chord length. The blue lines in Fig. 1 (a)-(b) represent the baseline conditions when no actuators are switched on. It can be seen in Fig. 1 (a) that for α ranging from -6° to 16°, the different actuators globally increase the C_L of the airfoil model with a maximum improvement by the 3rd actuator of nearly 4 times the baseline value C_L = 0.0570 obtained at α = 0°. It can be seen that the 3rd actuator (green line) generates a higher lift coefficient compared to the other actuators at negative angles up to 0°, while the 2nd actuator (red line) produces the largest C_L for angles between 2° and 10°. At high angles of attack between 12° and 16°, the plasma generated from the 1st actuator (black line) produces the largest lift coefficient. For example at -6°, the 3rd actuator generates the highest lift coefficient with a value slightly more than 44 % the baseline value, while at 16°, the first actuator generates the best lift coefficient with an improvement of 75.7 % over the baseline value. Therefore, the position of the actuator associated with the best C_L gets closer to the leading edge with increasing values of α. Concerning the drag coefficient shown in Fig. 1 (b), the plasma generated by the 3rd actuator generates the lowest drag up to 4°, which is a slightly larger α range compared to that for which the same actuator generates the best lift in Fig. 1 (a). Up to 12° the airfoil has very similar drag coefficient when the plasma from the 2nd or the 1st actuator is switched on, for example C_D = 0.138 and 0.139 at 12° for the 1st and 2nd actuators, respectively. Above 12°, the drag is lower when the 1st actuator is turned on. The trend of the lift and drag generated by the 1st, 2nd and 3rd actuators are similar with approximately the same actuators generating the best lift or drag coefficients for the same range of angles of attack even if for some angles, the actuator producing the best lift may not necessarily be the actuator producing the lowest drag. As α increases, it can be noticed that the best lift and drag coefficients are obtained from actuators located closer to the leading edge in Fig. 1 (a)-(b).

3.2 Particle Image Velocimetry measurements

Flow-field velocity measurements have been conducted using a two-velocity-component PIV system in order to further investigate the lift and drag generated by the plasma from actuators at different streamwise locations. In particular we were interested to locate the points of separation above the airfoil by analyzing the PIV measurements. The goal is to study the relation between the actuator location producing the best lift coefficient and lowest drag coefficient established in part 3.1 and its distance to the point of separation. First, we aimed to locate the point of separation along the airfoil model without DBD actuation. PIV experiments at Re = 35000 for α ranging from -6° to 16° have been conducted. No detached flow was observed for angles below 0°, whereas for positive angles, the flow detached from the airfoil model. The method of calculation of the point of separation consists in finding the x-location where the streamwise velocity becomes negative at approximately 2.5 mm away from the airfoil model since PIV reflection closer to the model surface prevented finding accurately the position where the streamwise velocity component becomes negative. Once this point is found, a line through it perpendicular to the model surface is drawn to find the location of the point of separation on the airfoil. The evolution of the non-dimensional streamwise position of the point of separation with α is shown in Fig. 2. It can be noticed that the location of the point of separation is closer to the leading edge as α increases. For example, at 16°, the point of separation is located at $x = 0.31c$ while at 0°, the location is $x = 0.87c$. It is interesting to note that the points of separation are located between 30% of the chord and the trailing edge.

In the last part of the paper, we are interested to look at the distance between the points of separation discussed above and the position of the actuator to find whether there is a relation between these 2 locations and the lift or drag generated when the actuator is on. Figure 2 indicates that the flow only detaches only from 0° onward therefore PIV experiments when the actuators are switched on have been carried out only for positive values of α. Typical flow field velocity measurements and vorticity contours are shown

in Fig. 3 (a)-(d) at α =10° and *Re* = 35000. The flow detaches from the airfoil when none of the actuators is switched on, Fig. 3 (a). When the 1st and 2nd actuators are switched on (green rectangle) respectively in Fig. 3 (b)-(c), the flow is reattached, while the flow is still detached in Fig. 3 (d) when only the 3rd actuator is on (green rectangle). This trend is confirmed in Fig. 1 (a)-(b). From the latter figure, it can be found out that the plasma generated from the 1st and 2nd actuators improved the lift and drag coefficient of the baseline flow at α =10° while the plasma from the 3rd actuator barely improved it. In Fig. 4 (a)-(b), the evolutions of the non-dimensional curvilinear distances between the flow separation points and each of the actuator location with the angles are plotted for *Re* = 35000. In these figures, the black, red and green lines correspond to the distance between the 1st, 2nd and 3rd actuators and the separation point, respectively. Both Fig. 4 (a) and (b) show roughly the same trend. It can be noticed that at each angle, the first actuator in black is located the farthest from the separation point, then comes the second actuator in red and then finally the 3rd actuator in green. For example at 16° in Fig. 4 (a), the first actuator in black is located +0.329*c* ahead of the separation point while the second and third actuators are located at 0.027*c* and 0.359*c* behind the separation point, respectively. In Fig. 4 (a), the actuators producing the best C_L at each angle are shown with a dotted blue line while in Fig. 4 (b), the actuators producing the lowest C_D for each angle are shown with a dotted magenta line. It can be seen that with increasing angles of attack, actuators located closer to the leading edge are more effective. For example, at 0°, the third actuator produces the best lift coefficient in Fig. 4 (a) and the lowest drag coefficient in Fig. 4 (b) while at 6°, the second actuator produces the best C_L and the lowest C_D and finally at 16°, the best actuator is the first one. Figures 4 (a)-(b) clearly indicate that the actuators have to be in front of the separation point to produce the best improvement on the lift and the drag and that no actuators located within the detachment area ($s_{separation} - s_{act} < 0$) produce the best lift or drag. It can also be shown that the effect on the baseline lift and drag is clearly limited when the actuator is located well within the separation zone. For example in Fig. 1 (a)-(b), the plasma generated from the 2nd actuator has very small effect on the improvement of the baseline lift and drag at 16°. At that angle, the corresponding actuator is located 0.04*c* behind the separation point shown in Fig. 4 (a)-(b) with a red line.

PIV experiments have been carried out to establish the relation between the position of the actuator and the lift and drag generated when the actuators are switched on. It is observed that the actuators have to be located in front of the separation flow zone to reattach the flow and to improve notably the drag and lift of the airfoil. With increasing angles of attack, actuators needs to be located closer to the leading edge to achieve better improvement of the baseline lift and drag.

4. Conclusions

In this study, three DBD plasma actuators have been mounted on a NACA 4415 airfoil model respectively at the leading edge, 30% and 60% of the chord length. Force balance measurements and Particle Image Velocimetry experiments have been conducted at a Reynolds number of 35000 and for angles of attack ranging from -6° to 16°. It is observed that the plasma generated by the actuators can improve the lift and drag of the airfoil by reattaching its flow. For each angle of attack, the location of the separation point on the airfoil surface has been identified and its distance from the different actuators has been calculated. With increasing angles of attack, the best lift and drag are obtained from actuators located closer to the leading edge. It has also been shown that the actuator needs to be in front of the separation point to produce the best lift and drag. Actuators located within the separation flow zone have very limited effect on lift and drag.

References

[1] Moreau E, Airflow control by non-thermal plasma actuators, *Journal of Physics D: Applied Physics*, Vol. 40, pp. 605-636, 2007.

[2] Jolibois J, Forte M, Moreau E, Application of an AC barrier discharge actuator to control airflow separation above a NACA 0015 airfoil: Optimization of the actuation location along the chord, *Journal of Electrostatics*, Vol. 66, pp. 496-503, 2008.

[3] Little J, Nishihara M, Adamovich I, Samimy M, High-lift airfoil trailing edge separation control using a single dielectric barrier discharge plasma actuator, *Exp. Fluids*, Vol. 48, pp.521-537, 2010

[4] Zhang X, Luo X, Chen P, Airfoil Flow Control Using Plasma Actuation and Coanda Effect, *29th AIAA Applied Aerodynamics Conference 27 - 30 June 2011, Honolulu, Hawaii*, AIAA 2011-3516, 2011.

Appendices

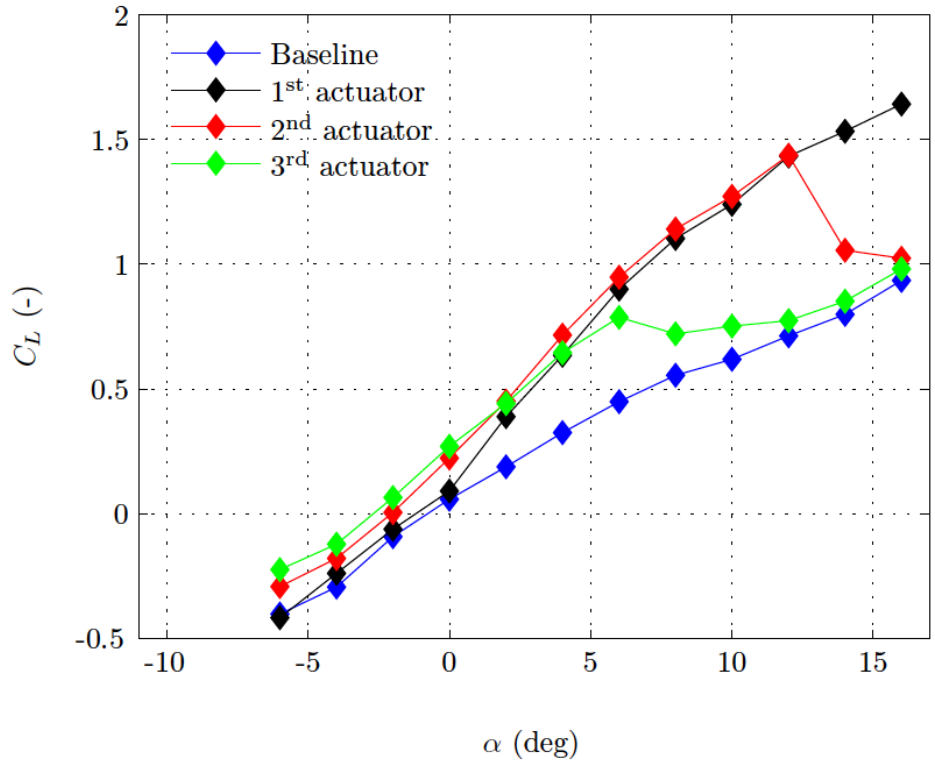

(a)

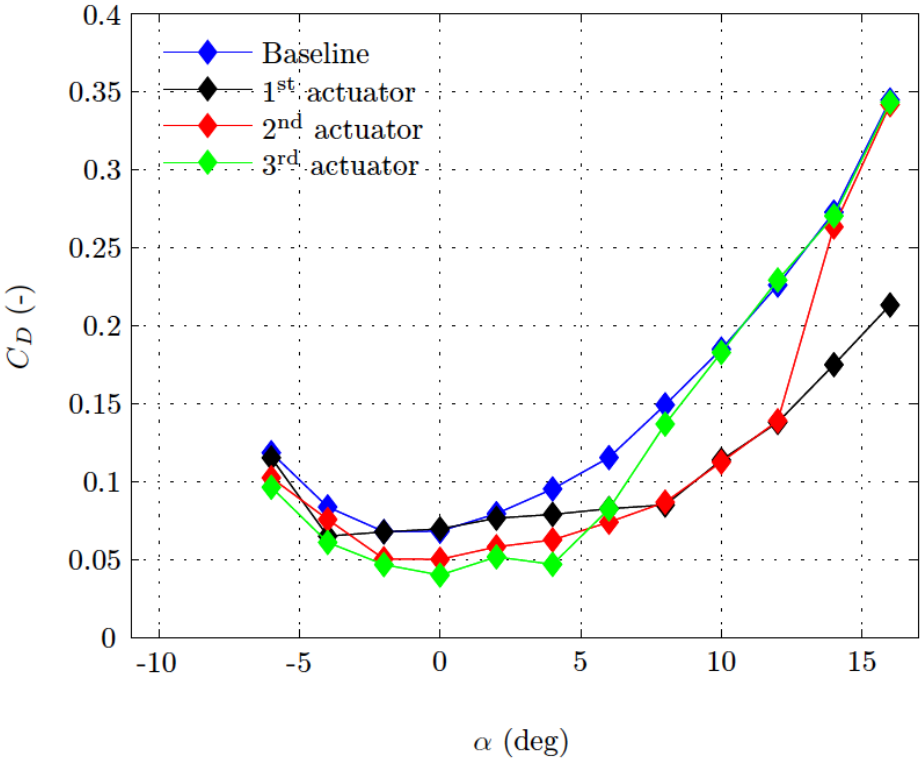

(b)

Fig.1 Variation of the lift coefficient and the drag coefficient with the angle of attack when the 1st, 2nd and 3rd actuators are switched on for *Re* = 35000: (a): C_L; (b): C_D.

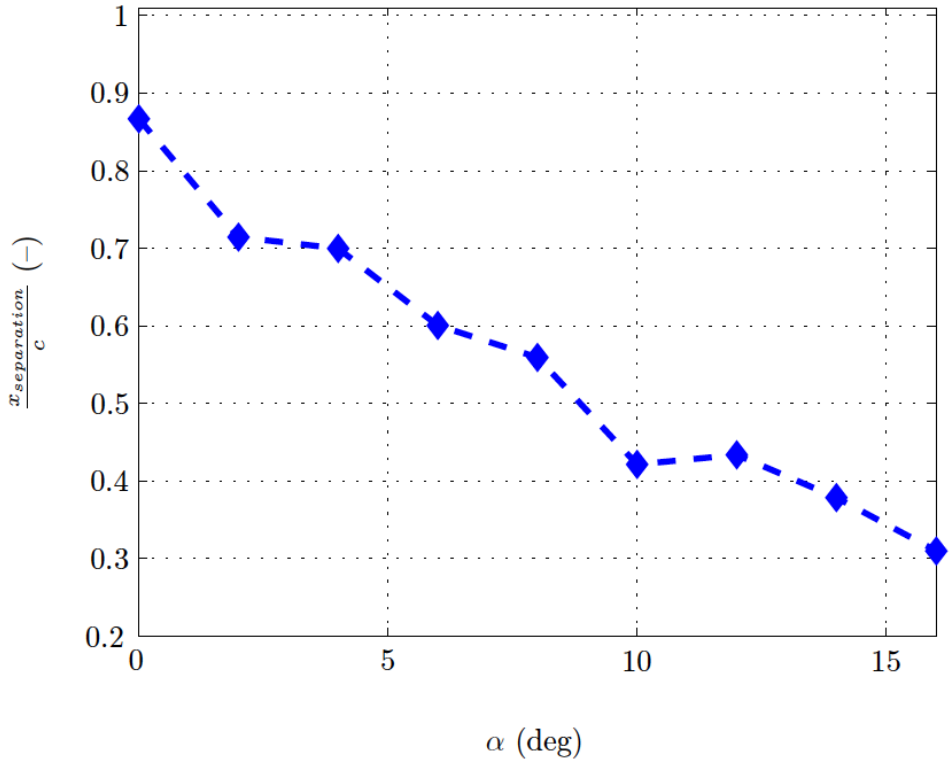

Fig. 2 Variation of the non-dimensional location of the separation point with the angle of attack for *Re* = 35000.

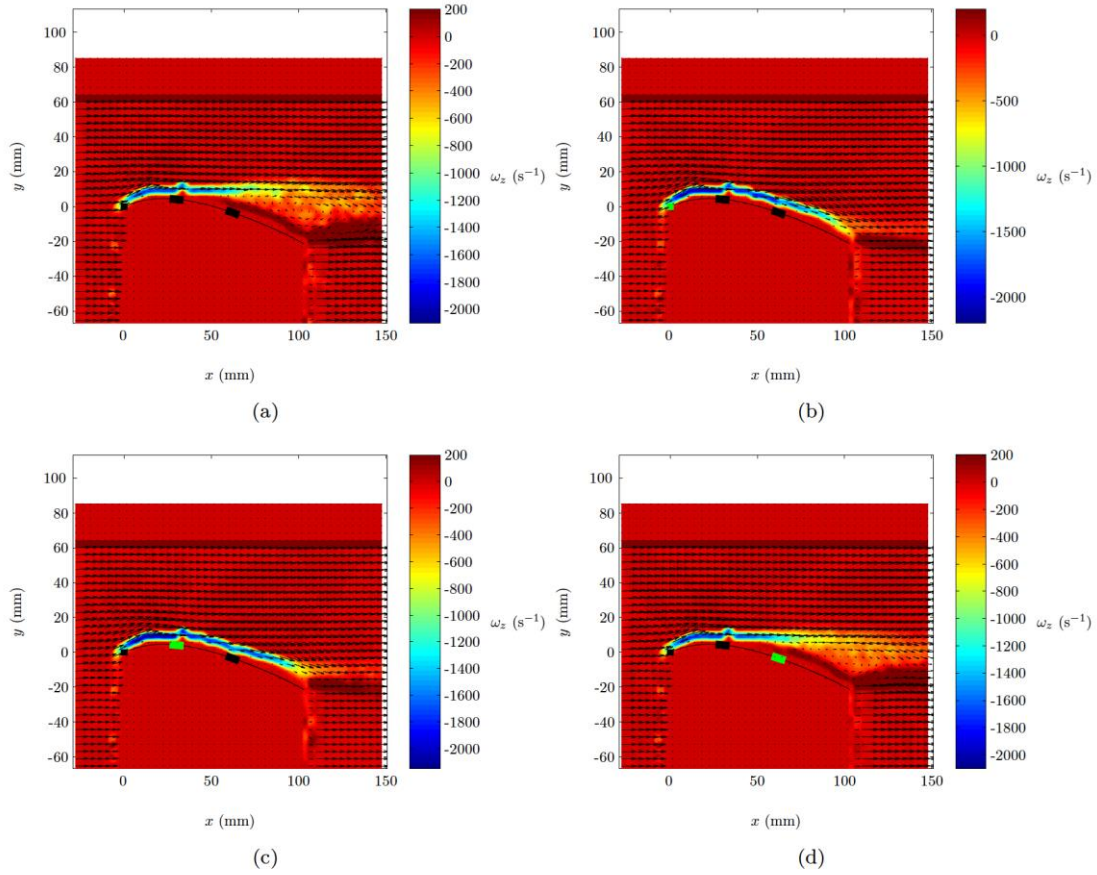

Fig. 3 Velocity vector and vorticity contour plots with the upper surface airfoil curvature and the actuators for an angle of attack of 10° and *Re* = 35000: (a): no actuation; (b): 1st actuator on (green rectangle); (c): 2nd actuator on (green rectangle); (d): 3rd actuator on (green rectangle).

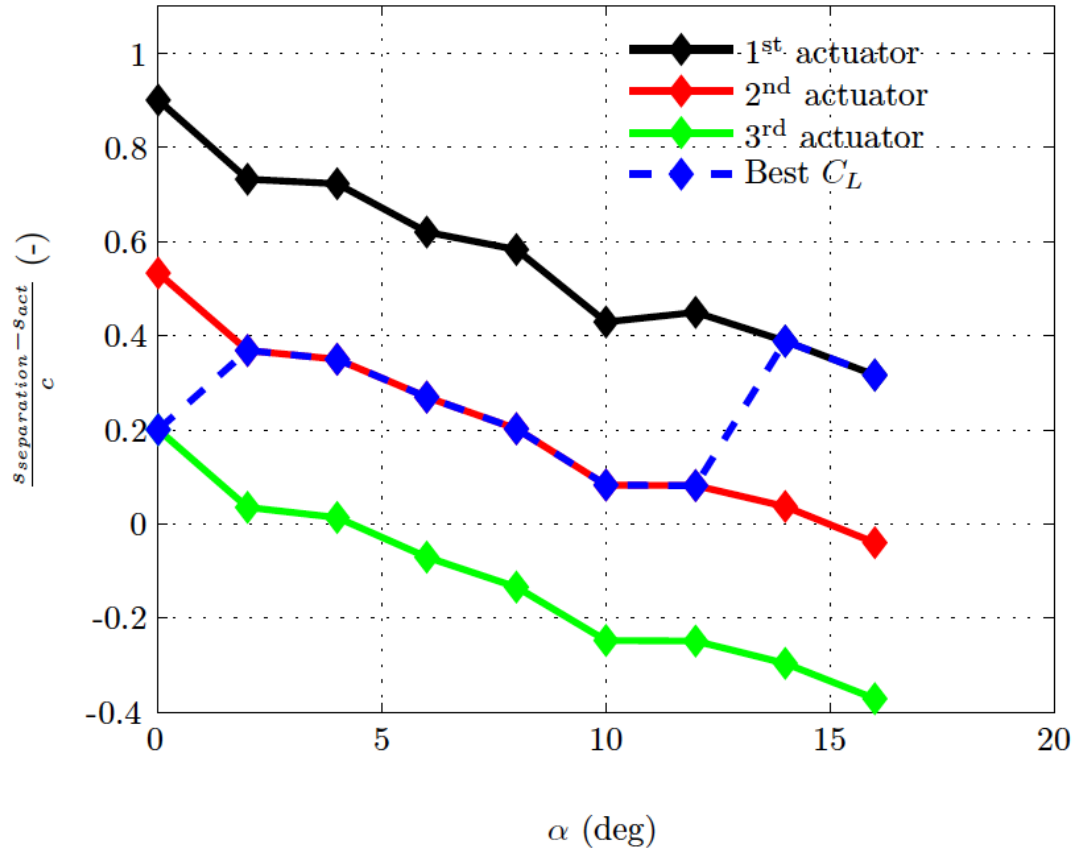

(a)

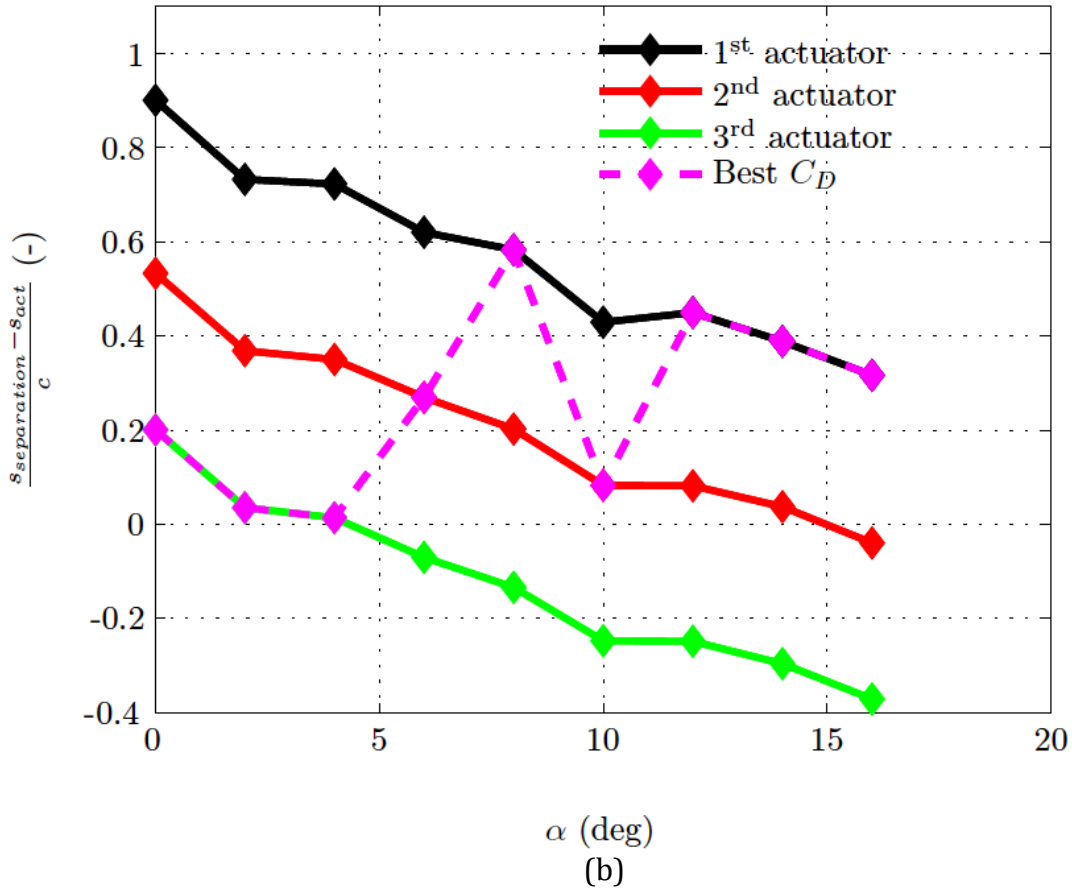

(b)

Fig. 4 Evolution of the non-dimensional curvilinear distances between the flow separation points and the actuator locations with the angle of attack for *Re* = 35000: (a): actuators associated with the best C_L underlined with a dotted blue line; (b): actuators associated with the best C_D underlined with a dotted magenta line.